Split-sideband spectroscopy in slowly modulated optomechanics

2016 New J. Phys. 18 113021

(http://iopscience.iop.org/1367-2630/18/11/113021)

New Journal of Physics
The open access journal at the forefront of physics

Deutsche Physikalische Gesellschaft DPG
IOP Institute of Physics

Published in partnership with: Deutsche Physikalische Gesellschaft and the Institute of Physics

OPEN ACCESS

RECEIVED
22 July 2016

REVISED
14 September 2016

ACCEPTED FOR PUBLICATION
18 October 2016

PUBLISHED
9 November 2016

PAPER

Split-sideband spectroscopy in slowly modulated optomechanics

E B Aranas, P Z G Fonseca, P F Barker and T S Monteiro[1]

Department of Physics and Astronomy, University College London, Gower Street, London WC1E 6BT, UK
[1] Author to whom any correspondence should be addressed.

E-mail: t.monteiro@ucl.ac.uk

Keywords: cavity optomechanics, levitated nanoparticles, quantum noise

Abstract

Optomechanical coupling between the motion of a mechanical oscillator and a cavity represents a new arena for experimental investigation of quantum effects on the mesoscopic and macroscopic scale. The motional sidebands of the output of a cavity offer ultra-sensitive probes of the dynamics. We introduce a scheme whereby these sidebands split asymmetrically and show how they may be used as experimental diagnostics and signatures of quantum noise limited dynamics. We show split-sidebands with controllable asymmetry occur by simultaneously modulating the light-mechanical coupling g and the mechanical frequency, $\omega_{\rm M}$—slowly and out-of-phase. Such modulations are generic but already occur in optically trapped set-ups where the equilibrium point of the oscillator is varied cyclically. We analyse recently observed, but overlooked, experimental split-sideband asymmetries; although not yet in the quantum regime, the data suggests that split sideband structures are easily accessible to future experiments.

1. Introduction

Cavity optomechanics offers rich possibilities for experimental investigation of the theory of quantum measurement and the role of quantum noise [1, 2]. Several groups have successfully cooled a mechanical oscillator via its coupling to a mode of an electromagnetic cavity [3–5] down to its quantum ground state (or very close to it) i.e. mean phonon occupancy $n_{\rm ph} \lesssim 1$. Read-out of the temperature was achieved by detection of motional sidebands in the cavity output; the theory for quantum sidebands was elucidated in [6, 7] . The cavity fields serve a dual purpose: they provide not only the laser cooling but also an ultrasensitive means for detection of displacements on the scale of quantum zero-point fluctuations; this has motivated considerable interest in quantum-limited measurements in this context, following the early pioneering work by Braginsky and Khalili [8].

An important development was the detection of an asymmetry [9–11] in the two frequency peaks (sidebands) of the output power of a probe beam detuned to the positive and negative side of the cavity resonance. Albeit indirectly [10, 11], the observations mirror an underlying asymmetry in the motional spectrum: an oscillator in its ground state $n_{\rm ph} = 0$, can absorb a phonon and down-convert the photon frequency (Stokes process); but it can no longer emit any energy and up-convert a photon (anti-Stokes process).

Sideband asymmetry has become an important tool in optomechanics and has now been used to establish cooling limited by only quantum backaction [12]. Ponderomotive squeezing, whereby narrowband cavity output falls below the technical imprecision noise floor is also of much current interest [13–15] though is also observed in oscillators in a high thermal state.

Recent rapid progress on cooling optically levitated systems suggests ground state cooling may be in sight [16–18]. This strongly motivates development of robust probes of the quantum dynamics. Such systems offer unique potential to sensitively probe quantum noises due to their near complete decoupling from environmental heating and decoherence. They also readily access the quantum shot-noise limit [17], since in a vacuum, the mechanical damping $\Gamma_{\rm M} \to 0$.

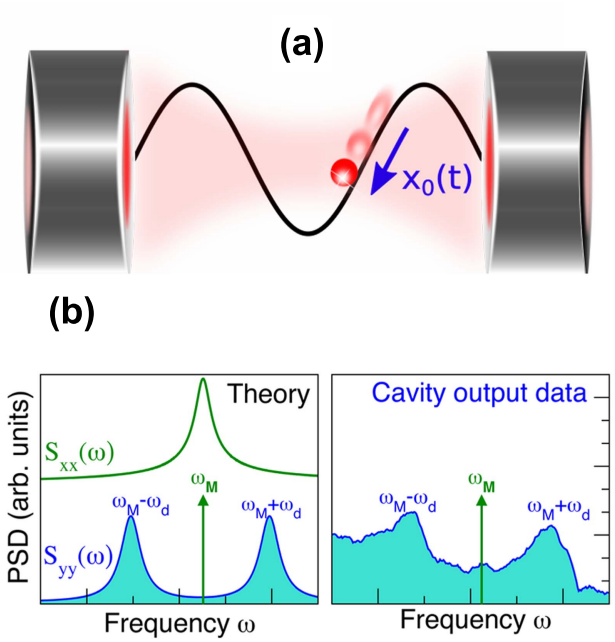

Figure 1. (a) An example of a modulated optomechanical system: for set-ups where an oscillator is dipole-force trapped by the standing wave of a cavity mode, there is no optomechanical cooling at the antinode $x_0 = 0$ (the potential minimum of an optical well of width $\lambda/2$), since there is no light–matter coupling. Hence, such set-ups [26, 29] require an auxiliary field to pull the centre of the mechanical oscillation away from $x_0 = 0$. In electro-optical traps [29], a slow oscillation is induced such that $x_0(t) = X_d \sin\omega_d t$, enabling cooling. For small oscillations, here we find this corresponds to an effective modulation of the optomechanical coupling $g(t) = 2\bar{g}\sin\omega_d t$ and a simultaneous, out-of-phase, modulation of the mechanical frequency $\omega_M(t) = \bar{\omega}_M + 2\omega_2\cos(2\omega_d t)$. (b) For a small ($X_d \ll \lambda$) modulation, $\omega_2 \approx 0$ and only g is appreciably modulated. In that case, while the power spectral density (PSD) of the displacement spectrum, $S_{xx}(\omega) \equiv \langle|\hat{X}(\omega)|^2\rangle$, is still peaked at $\pm\omega \simeq \omega_M$, the cavity spectrum, ($S_{yy}(\omega)$) exhibits a characteristic structure of 'twin peaks' at $\pm\omega = \omega_M \pm \omega_d$ (left panel). The measured cavity output spectrum (right panel) detected by a heterodyne method, also exhibits this behaviour.

A standard optomechanical system comprises a mechanical oscillator interacting with a laser-driven cavity. In the frame rotating with the driving laser, typical experimental regimes using an extraordinarily broad range of physical platforms (cantilevers, microtoroids, membranes, photonic crystals) are well described by the two-coupled oscillator Hamiltonian:

$$\hat{H}/\hbar = \Delta\hat{a}^\dagger\hat{a} + \omega_M(\hat{p}^2 + \hat{x}^2) + g(\hat{a}^\dagger + \hat{a})\hat{X}. \quad (1)$$

$\hat{a}^\dagger$, $\hat{a}$ are creation and annihilation operators for small fluctuations cavity mode about its equilibrium value α while $\hat{x} \equiv \hat{b} + \hat{b}^\dagger$ (in appropriately scaled units) represents a small displacement of the mechanical oscillator about its equilibrium position x_0. Dissipative processes are treated by standard input–output theory, including input noises incident in the optical cavity $\sqrt{\kappa}\,\hat{a}_{in}$, $\sqrt{\kappa}\,\hat{a}_{in}^\dagger$ and mechanical oscillator $\sqrt{\Gamma_M}\,\hat{b}_{in}$, $\sqrt{\Gamma_M}\,\hat{b}_{in}^\dagger$ where κ, Γ_M are the cavity and mechanical damping rates while g is the strength of the optomechanical coupling.

However, here we consider instead a harmonically modulated optomechanical coupling $g(t) = 2\bar{g}\sin\omega_d t$ and mechanical frequency $\omega_M(t) = \bar{\omega}_M + 2\omega_2\cos 2\omega_d t$. Other studies have investigated periodically modulated optomechanics, but interest has been focused on *resonant* driving $\omega_d \sim \omega_M$, $|\Delta|$ [19, 20] leading to interesting effects like squeezing or OMIT [21]. In contrast, here we investigate systems which are modulated slowly $\bar{\omega}_M \gg \omega_d$ (so as to preserve linearisation about $x_0(t)$ and α) and hence are far off-resonant. In addition, the g, ω_M modulations are out of phase, in the sense that when the mechanical frequency is a maximum, the magnitude of coupling strength between motion and cavity field is a minimum; and vice versa.

Added impetus to our study is provided by its relevance to optically trapped systems including levitated nanoparticles [22–28]. We show here that the anti-phase g, ω_M modulation arises automatically if the mean position of the oscillator varies harmonically $x_0(t) = X_d \sin\omega_d t$ as occurs for nanoparticles in hybrid electrical-optical traps [16, 29]. Such traps to date provide the only experimental realisation of stable trapping and cooling of a nanoparticle at high vacuum, in a cavity. This is illustrated in figure 1(b) where we also show that for these systems, the cavity output (lower panels, detected by a heterodyne method as in [16]) no longer has similar frequency spectrum to the displacement spectrum $S_{xx}(\omega) \equiv \langle|\hat{X}(\omega)|^2\rangle$ which is peaked at $\omega = \pm\omega_M$). In contrast, the cavity output modulations are peaked at frequencies $\omega = \omega_M \pm \omega_d$. The theory developed here accounts for this behaviour as well as unexplained asymmetries in the sidebands of levitated oscillators seen previously [29].

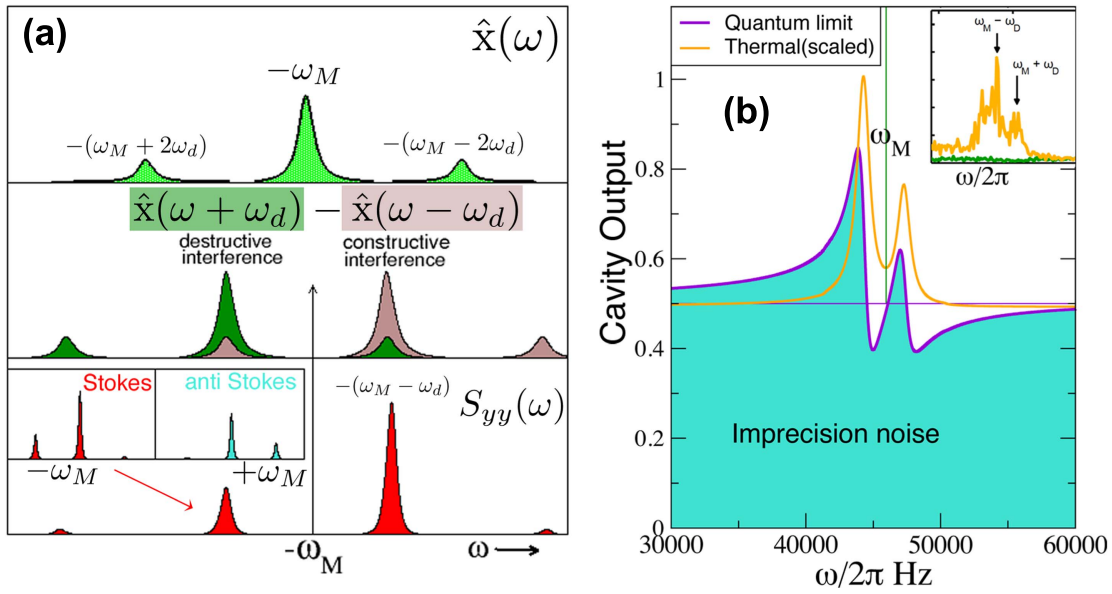

Figure 2. (a) For a generic system where both $g(t) = 2\bar{g}\sin\omega_d t$ and $\omega_M(t) = \bar{\omega}_M + 2\omega_2\cos 2\omega_d t$ are modulated, figure illustrates schematically how the spectrum of the cavity field ($S_{yy}(\omega)$), arises from the spectrum of the mechanical motion. Top panel illustrates the $\hat{X}(\omega)$ spectrum: the effect of $\omega_2 > 0$ is to produce additional $\pm 2\omega_d$ side-peaks. Middle panel: unlike the typical optomechanical case, the cavity field now follows $\hat{X}(\omega+\omega_d) - \hat{X}(\omega-\omega_d)$ rather than $\hat{X}(\omega)$. The interference of the individual $\hat{X}(\omega \pm \omega_d)$ components (shown in brown/green) yields constructive enhancement near $\omega \simeq \pm(\omega_M - \omega_d)$, and destructive cancellation near $\omega \simeq \pm(\omega_M + \omega_d)$. Instead of the 'twin peak' structure seen in figure 1 for $\omega_2 = 0$, the resultant cavity output sidebands display a pair of peaks of asymmetric heights (lower panel). For small $\bar{g}$, the ratio between peaks $r \simeq (\omega_2 - 2\omega_d)^2/(\omega_2 + 2\omega_d)^2$ so the $\omega_M + \omega_d$ peak is strongly suppressed for $\omega_2 \sim 2\omega_d$ ($r \approx 0$). This asymmetry is distinct from the usual Stokes/antiStokes sideband asymmetry at $\pm\omega \simeq \omega_M$, which is still present. Lower panel shows the Stokes peaks (red). (b) In thermal regimes, the ratio r is insensitive to Γ_M; however, as $\Gamma_M \to 0$ and the backaction limit is attained, correlations between back-action and incoming noise alters the relative heights of the peaks, mainly since ponderomotive squeezing lowers the height of the $\omega_M + \omega_d$ peak relative to the imprecision floor. For incoming quantum shot noise, significant changes in r arise only if the oscillator is near the ground state. Inset reproduces part of figure 5 of [29] illustrating previously overlooked asymmetries in experimental sidebands which supports our modulated-optomechanics model.

However, the key objective of the study is to investigate the dynamics, including the quantum spectra, of any set-up that can achieve these anti-phase g, ω_M modulations. Thus central parts of the study are generic to any system described by the optomechanics Hamiltonian equation (1), but with the additional g, ω_M modulations. In section 2 we present the theory. The results of section 2, in the appendix and in figures 2 and 3 are generic and make no reference to a specific set-up.

The analytical solutions are more challenging than for the standard case: unlike the former , where closed-form solutions are the norm, in the present case only approximate expressions are possible. Here we obtain solutions via an iterative method. Then in section 3, the derived expressions are tested and validated against numerical solutions, of the nonlinear stochastic equations of motion, developed previously to simulate data in [16, 29]. In the numerics, the values g and ω_M, including their modulation properties, are not even specified: they are simply emergent properties of the combined trapping fields. Here we exploit the fact that, when the particle is cold, the nonlinear Langevin numerics agree with linearised expressions, in the classical regime. The validated expressions can then be used to investigate quantum regimes by taking the $\Gamma_M \to 0$ limit. A comparison between the analytical expressions and the numerics is presented in figure 4.

2. Slowly modulated optomechanics

The equations of motion for the standard set-up equation (1) can be solved [1] in frequency space to obtain quantum spectra of experimental or theoretical interest . In terms of quadrature operators $\hat{y}(\omega) = \frac{1}{\sqrt{2}}(\hat{a}^\dagger(\omega) + \hat{a}(\omega))$ one obtains:

$$\hat{y}(\omega) = ig\eta(\omega)\cdot\hat{X}(\omega) + \sqrt{\kappa}\,\hat{Y}_{\rm th}(\omega), \tag{2}$$

where $\eta(\omega) = \chi_o(\omega) - \chi_o^*(-\omega)$ and $\hat{Y}_{\rm th}(\omega) = \chi_o(\omega)\hat{a}_{\rm in} + \chi_o^*(-\omega)\hat{a}_{\rm in}^\dagger$, while $\chi_o(\omega) = \left[-i(\omega+\Delta) + \frac{\kappa}{2}\right]^{-1}$ represents the optical susceptibility. In this well-known form, the first term represents the back-action of the mechanical motion on the cavity field, the second the cavity-filtered incoming quantum noise. The measurable, cavity output spectrum is then obtained from input–output theory [1] $\hat{a}_{\rm out}(\omega) = \hat{a}_{\rm in} - \sqrt{\kappa}\,\hat{a}(\omega)$ by considering

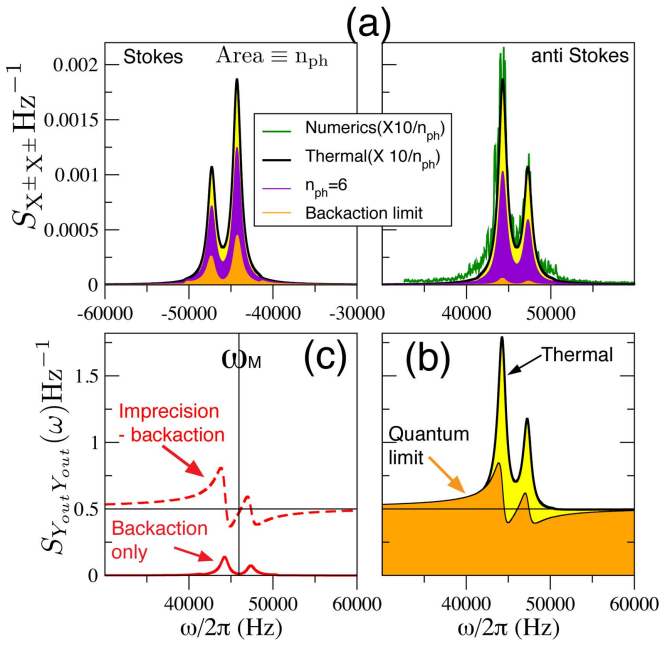

Figure 3. Comparison between the thermal spectrum and the quantum limit, using the analytical solutions with increasing g, ω_2 in the sideband-resolved limit, which can yield ground state cooling at sufficiently low pressures. (a) Shows $S_{X^{\pm}X^{\pm}}(\omega)$ for Stokes and anti-Stokes sidebands, as $\Gamma_{\rm M} \to 0$ while the optomechanical cooling rate $\Gamma_{\rm opt}$ in each graph remains fixed. The individual sideband shapes are unchanged, but Stokes/anti-Stokes asymmetry develops. The symmetric classical spectra are scaled to a height of 1 corresponding to $\Gamma_{\rm M} = 10^{-4}\,{\rm s}^{-1}$. $\omega_2/2\omega_{\rm d} = 0.24$, for $2\omega_{\rm d} = 3 \times 2\pi$ kHz; $g = 18\,500\,{\rm s}^{-1}$, $\bar{\omega}_{\rm M} = 46 \times 2\pi$ kHz, $\kappa/2 = 26 \times 2\pi$ kHz, $\Delta \simeq -\omega_{\rm M}$. (b) The same solutions in (b) are now added to incoming imprecision noise to obtain output spectra $S_{y_{\rm out}y_{\rm out}}(\omega)$. At high phonon occupancies, the shape is unchanged. As $n_{\rm ph} \to n_{\rm BA}$, the ratio above the quantum imprecision floor alters significantly. (c) Shows individual contributions to the PSD; the pure backaction term has the same shape as the thermal split sidebands; its interference with incoming imprecision noise lowers the height of the $\omega_{\rm M} + \omega_{\rm d}$ sideband.

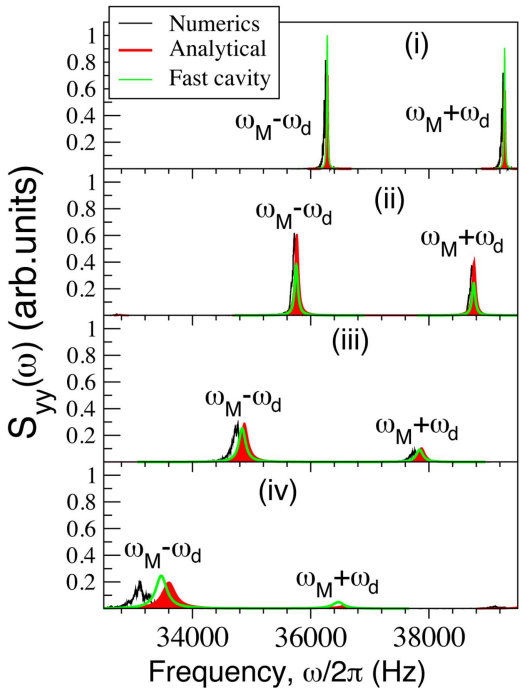

Figure 4. Comparison of the analytical split-sideband calculations with stochastic numerics and fast cavity model, with increasing $\bar{g}$, ω_2 for an optically trapped particle for thermal spectra, far from the quantum limit. Here, peak heights scale with $\Gamma_{\rm M}$ and r is independent of $\Gamma_{\rm M}$. In this regime, to obtain $S_{yy}(\omega)$ in units of ${\rm Hz}^{-1}$, for arbitrary $\Gamma_{\rm M}$, graphs should be scaled as $S_{yy}(\omega) \times \Gamma_{\rm M}/0.8$; in turn, for the optically trapped nanoparticles in [16], $\Gamma_{\rm M} \simeq 0.2 \times 10^4 P$, where the gas pressure ranges from $P = 1 - 10^{-8}$ mbar. $\kappa/2 = 130 \times 2\pi$ kHz, $\Delta \simeq -75 \times 2\pi$ kHz. Parameters are far from the sideband-resolved limit, so the fast-cavity model also gives reasonable results. $N = 100,\ 200,\ 300,\ 400$ in equation (10) hence (i) $\omega_2/2\omega_{\rm d} = 0.05$, $\bar{g} = 8500\ {\rm s}^{-1}$ (ii) $\omega_2/2\omega_{\rm d} = 0.2$, $\bar{g} = 17\,000\ {\rm s}^{-1}$ (iii) $\omega_2/2\omega_{\rm d} = 0.5$, $\bar{g} = 25\,000\ {\rm s}^{-1}$, (iv) $\omega_2/2\omega_{\rm d} = 0.9$, $\bar{g} = 33\,000\ {\rm s}^{-1}$.

the interference with the incoming (imprecision noise, typically shot noise from the laser), so $\hat{y}_{\rm out}(\omega) = \frac{1}{\sqrt{2}}[\hat{a}_{\rm out}(\omega) + \hat{a}^{\dagger}_{\rm out}(\omega)]$.

However, if we solve the equations of motion including the modulation of $g(t)$ we obtain instead:

$$\hat{y}(\omega) = \bar{g}\eta(\omega)\cdot[\hat{X}(\omega+\omega_{\rm d}) - \hat{X}(\omega-\omega_{\rm d})] + \sqrt{\kappa}\,\hat{Y}_{\rm th}(\omega). \tag{3}$$

We elucidate details in the appendix, but the notable difference between the standard case and the modulated optomechanics considered here is that in equation (3) the optical field does not probe the displacement spectrum $\hat{\rm x}(\omega)$ but is, instead, sensitive to the interference between the shifted displacement spectra at $\omega_{\rm M} \pm \omega_{\rm d}$.

For $\omega_2 \simeq 0$, the minus sign in equation (3) is not significant: the shifted spectra do not interfere appreciably. The result is a cavity field fluctuation spectrum characterised by a 'twin peaks' structure. However, the effect of the additional frequency modulation, $\omega_{\rm M}(t) = \bar{\omega}_{\rm M} + 2\omega_2\cos 2\omega_{\rm d}t$, is to couple $\hat{X}(\omega)$ directly to $\hat{X}(\omega \pm 2\omega_{\rm d})$; in that case, $\hat{X}(\omega)$ acquires corresponding sidebands which, as illustrated in figure 2(a), cause the two main peaks of the shifted spectra $\hat{X}^{\pm}(\omega) = \hat{X}(\omega+\omega_{\rm d}) - \hat{X}(\omega-\omega_{\rm d})$ to interfere with each other's sidebands. In this case, the minus sign in equation (3) (and the out-of-phase nature of the modulations) implies that one peak grows by constructive interference, while the other one diminishes.

Further details are in the appendix, but this can be understood from a simple argument. For modest backaction ($\bar{g}$ small), we can write $\hat{X}^{\pm}(\omega)$ in the form:

$$\begin{aligned}\hat{X}^{\pm}(\omega) \;\approx\; & \sqrt{\Gamma_{\rm M}}\,[\hat{X}_{\rm th}(\omega+\omega_{\rm d}) - \hat{X}_{\rm th}(\omega-\omega_{\rm d})] \\ & + \bar{g}\hat{Y}_{\rm BA}(\omega) - {\rm i}\omega_2\sqrt{\Gamma_{\rm M}}\hat{X}_{\omega_2}(\omega) - {\rm i}\omega_2\bar{g}\hat{Y}^{(\omega_2)}_{\rm BA}(\omega),\end{aligned} \tag{4}$$

where the $\hat{X}_{\rm th}$ terms represent incoming thermal noises, $\hat{Y}_{\rm BA}$ represents the back-action terms driven by imprecision noise. The last two terms are corrections to account for the modulation of $\omega_{\rm M}$; the first comprises thermal effects, the second the corresponding back-action effects.

For $\omega_2 = 0$ and neglecting backaction, the shifted spectra arise mainly from incoming thermal noises $\hat{X}_{\rm th}(\omega) = \chi_{\rm M}(\omega)\hat{b}_{\rm in} + \chi^{*}_{\rm M}(-\omega)\hat{b}^{\dagger}_{\rm in}$ weighted by the mechanical susceptibility $\chi_{\rm M}(\omega) = \left[-{\rm i}(\omega-\omega_{\rm M}) + \frac{\Gamma_{\rm M}}{2}\right]^{-1}$. The anti-Stokes sideband for example, is primarily due to the weighted thermal noise operators $\chi_{\rm M}(\omega\pm\omega_{\rm d})\hat{b}_{\rm in}(\omega\pm\omega_{\rm d})$. The susceptibilities $|\chi_{\rm M}(\omega\pm\omega_{\rm d})|$ are sharply peaked at frequencies $\omega = \omega_{\rm M} \mp \omega_{\rm d}$ (since $\Gamma_{\rm M}$ is small), yielding the 'twin peaks' structure since the ratio of the twin peak weights $r = |\chi_{\rm M}(\omega-\omega_{\rm d})|^2/|\chi_{\rm M}(\omega+\omega_{\rm d})|^2 = 1$.

The main effect of ω_2 is to introduce the extra correction from the $\hat{X}_{\omega_2}$ term which means replacing the thermal weights:

$$\chi_{\rm M}(\omega\pm\omega_{\rm d}) \to \chi_{\rm M}(\omega\pm\omega_{\rm d})[1 - {\rm i}\omega_2\chi_{\rm M}(\omega\mp\omega_{\rm d})]. \tag{5}$$

Evaluating the corrections (the terms in square brackets) near the frequency peaks of the noise, we find they are $\approx(2\omega_{\rm d}\pm\omega_2)/2\omega_{\rm d}$ so the ratio of peaks in the PSD would be:

$$r \approx (2\omega_{\rm d}-\omega_2)^2/(2\omega_{\rm d}+\omega_2)^2, \tag{6}$$

predicting a full cancellation for $2\omega_{\rm d} \sim \omega_2$.

For the standard optomechanical equations, equation (2) and its $\hat{X}(\omega)$ equivalent are solved to obtain $S_{xx}(\omega)$ and $S_{yy}(\omega)$ or $S_{y_{\rm out}y_{\rm out}}(\omega)$ in closed form. However, for the modulated spectra this is not possible: $\hat{y}(\omega)$ depends on shifted $\hat{X}(\omega)$ spectra; and the ω_2 modulation couples $\hat{\rm x}(\omega)$ spectra to the displacement spectra $\hat{X}(\omega\pm2\omega_{\rm d})$. Equations (3) and (4) are instead solved iteratively, assuming $\bar{g}$, $\omega_2 \ll \kappa$, $\omega_{\rm M}$ and retaining terms up to quadratic order in $\bar{g}$, ω_2 (see appendix). In the thermal regime, the resulting equations can be shown to be accurate by testing against numerical stochastic equations, and another 'fast cavity' model, used to simulate optically trapped particles [16, 29], as seen in figure 4.

We then take $\Gamma_{\rm M} \to 0$ which for cooling parameters (red-detuned light) takes the system down to the quantum backaction limit, where the heating is limited by quantum shot noise, $n_{\rm ph} \equiv n_{\rm BA} \approx \left(\frac{\kappa}{4\omega_{\rm M}}\right)^2$ [12]. When we calculate $S_{X^{\pm}X^{\pm}}$ (the PSD for $\hat{X}^{\pm}(\omega)$), we find that it differs very little from the thermal spectrum. This indicates that even for $\Gamma_{\rm M} = 0$, (where the oscillator motion is completely driven by the incoming optical imprecision noise, quantum or classical), the shape, and r for $S_{X^{\pm}X^{\pm}}$ unchanged as shown in figure 3(a).

However, for $S_{y_{\rm out}y_{\rm out}}(\omega)$, this is not the case: when the same solution used for figure 3(a) is added and interfered with the incoming (imprecision) optical shot noise, the sideband shape is unchanged for the thermal regime but changes significantly in the quantum back-action limit.

The underlying reason for this change can be understood as follows: the total back-action in equation (4), $\bar{g}\hat{Y}_T(\omega) = \bar{g}[\hat{Y}_{\rm BA}(\omega) - {\rm i}\omega_2\hat{Y}^{(\omega_2)}_{\rm BA}(\omega)]$, which by itself still yields a ratio of r, develops correlations with the incoming imprecision terms $\hat{Y}_{\rm imp}(\omega) = \hat{a}_{\rm in} + \hat{a}^{\dagger}_{\rm in} - \sqrt{\kappa}\,\hat{Y}_{\rm th}$. The key difference seen between $S_{X^{\pm}X^{\pm}}$ and

$S_{y_{\rm out}y_{\rm out}}(\omega)$ in the quantum limit, arise because:

$$\langle|\bar{g}\hat{Y}_T(\omega)|^2\rangle \neq \left\langle\left|\frac{\hat{Y}_{\rm imp}(\omega)}{\sqrt{\kappa}} - \bar{g}\hat{Y}_T(\omega)\right|^2\right\rangle. \tag{7}$$

The above two terms are contrasted in figure 3(c). Ponderomotive squeezing originates from such correlations [13–15] between backaction and incoming noise and, in the standard optomechanical case, it leads to a Fano-like line experimental profile [13–15] and (an often small) dip where the output light spectrum lies below the imprecision floor.

However, in the present case, the height of the $\omega_{\rm M}+\omega_{\rm d}$ peak is lowered as it overlaps with a ponderomotive squeezing 'dip' of the stronger peak as seen in figure 3(b), leading to a change in r: the sideband structure is more strikingly reshaped and the $\Gamma_{\rm M}$ invariance of r is lost. Although ponderomotive squeezing does not require a ground state oscillator, for quantum shot-noise limited spectra, a change in r only becomes appreciable if $n_{\rm ph}\rightarrow n_{\rm BA}$, leading to a noticeable decrease in height of the $\omega_{\rm M}+\omega_{\rm d}$ peak above the imprecision noise level.

3. Comparisons with stochastic numerical model

One may test the validity and accuracy of the generic expressions derived above by comparing the calculated spectra with numerical solutions of equations of motion for the specific example of a levitated nanoparticle in a hybrid trap [16, 29] since, when linearised, they reduce to the modulated optomechanics case. Provided the particle motion $x(t)$ corresponds to small oscillations about an equilibrium value x_0 (which may be slowly modulated) and the cavity field dynamics $a(t)$ correspond to small fluctuations about a mean field α, comparisons are possible.

As outlined in [16, 29], a nanoparticle in a hybrid electrical-optical trap experiences a dipole force potential $V(x)=-\hbar A|a(t)|^2\cos^2(kx)$ from the optical standing wave of a cavity (with axis along x). In [16], the depth of the potential $A=26\times 2\pi$ kHz. In the equations of motion, the particle's motion causes an effective change in the length of the cavity by modifying the detuning between the driving laser and the cavity resonance:

$$\Delta(t)=\Delta+A\cos^2 kx(t). \tag{8}$$

Neglecting noise, the intracavity field $a(t)$ then is:

$$a(t)\approx\frac{\mathcal{E}_T}{(\mathrm{i}\Delta(t)+\kappa/2)}, \tag{9}$$

where $\mathcal{E}_T$ is the laser drive amplitude.

The cavity photon number $|a(t)|^2$ typically fluctuates about a mean value of $|\alpha|^2\approx 10^9$–10^{10} photons; $k=2\pi/\lambda$ with $\lambda=1064$ nm. The particle becomes trapped in a given optical well N, with anti-node (potential minimum) at $x=X_N$ where $2kX_N=2\pi N$. It experiences also an additional oscillating harmonic potential $V^{\rm AC}(x,t)=\frac{1}{2}m\omega_T^2(x+\mathrm{x}_N)^2\cos(\omega_{\rm d}t)$ from an ion trap, whose effect is to (relatively slowly) modulate $x_0(t)$.

We test our model by comparing with solutions of the equations of motion in these combined potentials, including also damping for the cavity (κ) and for mechanical degrees of freedom ($\Gamma_{\rm M}$) as well as stochastic Gaussian noise to allow for gas collisions and shot noise. This represents a stringent test of our analytical noise model since, in the numerics, $\bar{g}$, $\omega_{\rm M}$ and ω_2 are not even input parameters: they are themselves emergent properties of the numerical simulations. In the linearised regime we obtain (taking α to be real):

$$\begin{aligned} 2kx_0(t)&\approx-\frac{\omega_T^2}{\omega_{\rm M}^2}(2k\mathrm{x}_N)\sin(\omega_{\rm d}t)\equiv X_{\rm d}\sin(\omega_{\rm d}t),\\ m\omega_{\rm M}^2&=2\hbar k^2A\alpha^2\cos(2kx_0),\\ 2\bar{g}&=kA\alpha\sin(2kx_0). \end{aligned} \tag{10}$$

Hence the equilibrium point of the oscillations $x_0(t)$ oscillates as $\sin(\omega_{\rm d}t)$, leading to modulated $\omega_{\rm M}$, $\bar{g}$; analysis of the spring constant above yields the behaviour $\omega_{\rm M}\approx\overline{\omega}_{\rm M}+2\omega_2\cos 2\omega_{\rm d}t$.

However, solving the full stochastic nonlinear Langevin equations are laborious. Thus we note that in the fast cavity limit $\kappa\gg\omega_{\rm M}$, there is a simpler alternative model. Taylor expanding equation (9), one can easily show that $y(t)\propto\cos 2kx(t)$. For a fast cavity, we can assume the fluctuations of the cavity field follow $\cos 2kx(t)$ with no delay. In turn, $x(t)$ combines the slow $x_0(t)$ motion with the fast mechanical motion $X_{\rm M}(t)\simeq X_{\rm M}\cos\Phi_{\rm M}(t)$ where $X_{\rm M}$ is the variance of the thermal motion, the accumulated phase being $\Phi_{\rm M}(t)=\int_0^t\omega_{\rm M}(t')\,\mathrm{d}t'=\int_0^t(\overline{\omega}_{\rm M}+2\omega_2\cos 2\omega_{\rm d}t')\mathrm{d}t'$. Hence, $x(t)\simeq \mathrm{X}_{\rm d}\sin(\omega_{\rm d}t)+\mathrm{X}_{\rm M}\cos(\overline{\omega}_{\rm M}t+\frac{2\omega_2}{2\omega_{\rm d}}\sin 2\omega_{\rm d}t)$. We find the Fourier transform of $\cos 2kx(t)$ using this ansatz gives a reasonable approximation of the split-sideband spectrum for a fast cavity.

Figure 4, corresponding to $\kappa \gg \omega_M$, shows that it yields reasonable agreement with numerics and analysis. More importantly, it describes also scattering of light out of the cavity (illustrated in inset of figure 2(b)) which illustrated suppression of the $\omega_M + \omega_d$ sideband. While not a full demonstration, this classical-regime data does demonstrate the coherent relative phase accumulation and interplay between the slow and fast motions; it indicates that in combination with homodyne or heterodyne detection, split sideband asymmetries may be investigated experimentally once quantum-limited regimes are attained.

4. Conclusions

In the present paper we have obtained approximate analytical expressions for an optomechanical system subjected to slow, out-of-phase modulation of the optomechanical coupling and spring constant. We show that a generic feature that emerges are split-sidebands in the cavity output spectra: these sidebands are characterised by a dominant pair of peaks of unequal heights. The ratio of the peaks depends on the modulation amplitude. The shape of these structures remains invariant in the thermal regime, as Γ_M is reduced by many orders of magnitude, but changes shape significantly as the quantum-backation limited regime is attained.

Hence split sideband spectroscopy offers potential new experimental signatures of the underlying dynamics and also of the quantum regime; measurement of the ratio r complements Stokes/antiStokes asymmetry between the ω_M sidebands; it may be combined with that measurement to provide a more reliable quantum signature, since r is well defined and controllable and there is a sharp change in the quantum back-action limit; the double-sidebands may offer an additional diagnostic of Stokes/antiStokes asymmetry as there are two pairs of peaks to compare. It also offers a distinctive alternative experimental probe of ponderomotive squeezing; future studies will investigate whether these may be enhanced with modified techniques of detection (homodyne or general-dyne).

The expressions were tested and validated against stochastic numerics used to simulate current experiments on levitated nanoparticles in hybrid cavity-Paul trap setups. The optomechanical model is valid in both classical and quantum regimes and is shown here to accounts for previously unexplained split-sideband structures already seen in existing experiments.

Appendix. Calculation of noise spectra

Standard optomechanics

The Hamiltonian for an optomechanical system:

$$\hat{H}/\hbar = \Delta \hat{a}^\dagger \hat{a} + \frac{\hat{p}^2}{2m} + \frac{1}{2} m\omega_M^2 \hat{X}^2 + g\,(\hat{a}^\dagger + \hat{a})\hat{X} \tag{11}$$

leads to the following equations of motion, [1], describing the motion of two coupled harmonic oscillators:

$$\begin{aligned} \dot{\hat{b}} &= -\left(i\omega_M + \frac{\Gamma_M}{2}\right)\hat{b} + ig\,(\hat{a} + \hat{a}^\dagger) + \sqrt{\Gamma_M}\,\hat{b}_{in}, \\ \dot{\hat{a}} &= \left(i\Delta - \frac{\kappa}{2}\right)\hat{a} + ig\alpha(\hat{b} + \hat{b}^\dagger) + \sqrt{\kappa}\,\hat{a}_{in}, \end{aligned} \tag{12}$$

where the operators $\hat{a}(t) \to \alpha + \hat{a}(t)$, and $\hat{X} \to x_0 + \hat{X}(t)$ describe small displacements about an equilibrium cavity field α and the equilibrium position of the oscillator. The oscillators are characterised by a mechanical frequency ω_M and a detuning Δ from the cavity resonance frequency (since the Hamiltonian is given in a frame rotating at the laser frequency). In general, Δ includes a correction term dependent on x_0 (see below).

While $\hat{a}^\dagger$ and $\hat{a}$ are creation and annihilation operators for small fluctuations cavity mode, in the equations of motion we give $\hat{x}$ in operator form, thus $\hat{X} = \hat{b} + \hat{b}^\dagger$ (in the usual scaling $\hat{X} = X_{zpf}(\hat{b} + \hat{b}^\dagger)$ but here, for convenience, the appropriate length scaling $X_{zpf} = \sqrt{\hbar/(2m\omega_M)}$ is absorbed into g).

The equations of motion include dissipative terms given by standard input–output theory. κ, Γ_M are the cavity and mechanical damping rates. For the optical modes, this is laser noise incident in the optical cavity $\sqrt{\kappa}\,\hat{a}_{in}$, $\sqrt{\kappa}\,\hat{a}_{in}^\dagger$. We consider a single-sided cavity here; our results can be adapted to other configurations but are not modified qualitatively. The mechanical modes are subject to thermal noises which input incoming phonons. For the specific case of an optically trapped system, this is Brownian noise [16, 25, 26] from collisions with room-temperature gas molecules in the cavity, which in that case, depend on gas pressure P.

For the photon noise bath , we take the correlators

$$\langle \hat{a}_{\rm in}(t')\hat{a}^{\dagger}{}_{\rm in}(t)\rangle = (\bar{n}_a + 1)\delta(t - t'),$$
$$\langle \hat{a}^{\dagger}_{\rm in}(t')\hat{a}_{\rm in}(t)\rangle = \bar{n}_a\ \delta(t - t'), \tag{13}$$

where for photon shot noise, $\bar{n}_a = 0$. However we can also include a finite photon temperature to test for the effects of laser noise. For the thermal noises we take the bath

$$\langle \hat{b}_{\rm in}(t')\hat{b}^{\dagger}_{\rm in}(t)\rangle = (\bar{n}_b + 1)\delta(t - t'),$$
$$\langle \hat{b}^{\dagger}_{\rm in}(t')\hat{b}_{\rm in}(t)\rangle = \bar{n}_b\delta(t - t'), \tag{14}$$

where we approximate the number of surrounding bath phonons as $\bar{n}_b \approx \frac{k_B T}{\hbar\omega_{\rm M}}$. We note that for optical trapping experiments $T_B \simeq 300$ K, thus unlike cryogenically cooled experiments, thermal bath occupancy is extremely high $\bar{n}_b \sim 10^7$–10^8. However as the gas is pumped out to ulta-high vacuum, $\Gamma_{\rm M} \to 0$ and ground state cooling is possible.

The equations of motion are solved in frequency space. In terms of the position quadrature operators $\hat{y} = \frac{1}{\sqrt{2}}(\hat{a} + \hat{a}^{\dagger})$ and $\hat{x} = (\hat{b} + \hat{b}^{\dagger})$ one obtains [1]:

$$\hat{y}(\omega) = {\rm i}g\eta(\omega)\cdot\hat{X}(\omega) + \sqrt{\kappa}\,\hat{Y}_{\rm in}(\omega),$$
$$\hat{X}(\omega) = {\rm i}g\mu(\omega)\cdot\hat{y}(\omega) + \sqrt{\Gamma_{\rm M}}\hat{X}_{\rm th}(\omega) \tag{15}$$

where

$$\hat{Y}_{\rm in}(\omega) = \chi_o(\omega)\hat{a}_{\rm in} + \chi^{*}_o(-\omega)\hat{a}^{\dagger}_{\rm in},$$
$$\hat{X}_{\rm th}(\omega) = \chi_{\rm M}(\omega)\hat{b}_{\rm in} + \chi^{*}_{\rm M}(-\omega)\hat{b}^{\dagger}_{\rm in} \tag{16}$$

are operators combining incoming optical and thermal noise contributions, respectively, in convenient form. We use also the functions $\eta(\omega) = \chi_o(\omega) - \chi^{*}_o(-\omega)$ and $\mu(\omega) = \chi_{\rm M}(\omega) - \chi^{*}_{\rm M}(-\omega)$, given in terms of the usual optical susceptibility $\chi_o(\omega) = \left[-{\rm i}(\omega + \Delta) + \frac{\kappa}{2}\right]^{-1}$ and mechanical susceptibility $\chi_{\rm M}(\omega) = \left[-{\rm i}(\omega - \omega_{\rm M}) + \frac{\Gamma_{\rm M}}{2}\right]^{-1}$ respectively.

In order to calculate power spectral densities (PSDs) of either the displacement or the cavity fields, one re-expresses the operators equation (15) in terms of noise vectors, thus for example:

$$\hat{y}(\omega) = \vec{\mathcal{A}}_y(\omega)\cdot\vec{\mathcal{Z}}, \tag{17}$$

where $\vec{\mathcal{Z}} \equiv (\hat{b}_{\rm in}(\omega),\ b^{\dagger}_{\rm in}(\omega),\ \hat{a}_{\rm in}(\omega),\ \hat{a}^{\dagger}_{\rm in}(\omega))$ is a vector comprising the noise terms and where:

$$\vec{\mathcal{A}}_y(\omega) = (\mathcal{A}_b(\omega),\ \mathcal{A}_{b^{\dagger}}(\omega),\ \mathcal{A}_a(\omega),\ \mathcal{A}_{a^{\dagger}}(\omega)) \tag{18}$$

represents the respective coefficients at a given frequency ω.

The corresponding PSD relevant to heterodyne linear detection of the cavity field is hence:

$$S_{yy}(\omega) = \langle \hat{y}^{\dagger}(\omega)\hat{y}(\omega)\rangle \tag{19}$$

is then directly obtained from the noises using the correlators in equations (13) and (14). We note that for experimental analysis, a symmetrised version of equation (19) is typically evaluated [11]. As this does not affect our conclusions, we consider simply the unsymmetrised two-sided $S_{yy}(\omega)$.

Slowly modulated optomechanics

We now generalise to the case where g, $\omega_{\rm M}$ are now modulated, but sufficiently slowly $\omega_{\rm d} \ll \omega_{\rm M}$ so that linearisation about equilibrium is still possible; we consider a harmonically modulated optomechanical coupling $g(t) = 2\bar{g}\sin\omega_{\rm d}t$ as well as a modulated mechanical frequency $\omega_{\rm M}(t) = \overline{\omega}_{\rm M} + 2\omega_2\cos 2\omega_{\rm d}t$.

Introducing the g and $\omega_{\rm M}$ modulations in equation (12), the corresponding Fourier-transformed spectra become:

$$\hat{y}(\omega) = \bar{g}\eta(\omega)\cdot[\hat{X}(\omega + \omega_{\rm d}) - \hat{X}(\omega - \omega_{\rm d})] + \sqrt{\kappa}\,\hat{Y}_{\rm in}(\omega). \tag{20}$$

In other words, the optical field does not directly probe the mechanical motion but rather is sensitive to the difference between the displacement spectra at $\omega_{\rm M} \pm \omega_{\rm d}$. Conversely, the displacement spectrum is now:

$$\begin{aligned}\hat{X}(\omega) \ =\ & \bar{g}\mu(\omega)\cdot(\hat{y}(\omega + \omega_{\rm d}) - \hat{y}(\omega - \omega_{\rm d})) + \sqrt{\Gamma_{\rm M}}\hat{X}_{\rm th}(\omega)\\ & - {\rm i}\omega_2\mathcal{G}(\omega)\end{aligned} \tag{21}$$

with a similar dependence on shifted spectra. However, in this case there is also a correction due to the frequency modulation:

$$\begin{aligned}\mathcal{G}(\omega) &= \chi_{\rm M}(\omega)\{\hat{b}(\omega+2\omega_{\rm d})+\hat{b}(\omega-2\omega_{\rm d})\}\\ &\quad-\chi^{*}_{\rm M}(-\omega)\{\hat{b}^{\dagger}(\omega+2\omega_{\rm d})+\hat{b}^{\dagger}(\omega-2\omega_{\rm d})\}.\end{aligned} \tag{22}$$

Unlike the standard case, equations (20) and (21) can no longer be solved in closed form. We can however solve them iteratively, in a perturbative regime where $\omega_2 \ll \omega_{\rm d}$ and also for modest values of the coupling $g \ll \kappa,\ \omega_{\rm M}$. The latter condition implies back-action terms are not too large. Although we investigate here the case where a single mode is used for both cooling and read-out, in general, experiments will involve two modes, one for trapping/cooling, while a weaker probe field is used for read-out. The probe mode will have a much lower α so much smaller g. In the present case we restrict ourselves to values of g which are not too large. In this case, iterative substitution of equations (20) and (21) leads to expressions relating $\hat{X}(\omega)$ to terms shifted by the harmonics of the drive frequency $\hat{X}(\omega \pm n\omega_{\rm d})$ where $(n = 0,\ 1,\ 2,...)$. Here we truncate at $n \leqslant 2$.

Spectrum of shifted-displacement $\hat{X}^{\pm}(\omega)$

In this section we give explicit solutions for the shifted displacement spectrum:

$$\hat{X}^{\pm}(\omega) = \hat{X}(\omega+\omega_{\rm d}) - \hat{X}(\omega-\omega_{\rm d}) \tag{23}$$

since to obtain the intracavity spectrum, $\hat{y}(\omega)$ we simply need to interfere this with the cavity-filtered incoming noise term $\hat{Y}_{\rm in}(\omega)$. From this, the cavity output (relevant to for example heterodyne detection) can easily be obtained.

We can also include terms in ω_2^2, but have found that their effect in our spectra is not significant, so we do not present them here.

Hence we solve for $\hat{X}^{\pm}(\omega)$ up to *quadratic* order in $g,\ \omega_2$ (i.e. retaining terms in $g^2,\ g\omega_2$). We obtain, to a good approximation, the vector of noises analogous to equation (17):

$$\hat{X}^{\pm}(\omega) \simeq \vec{\mathcal{A}}_{X^{\pm}}(\omega)\cdot\mathcal{Z}_{\rm mod}(\omega), \tag{24}$$

noting that the noises vector in this case, $\mathcal{Z}_{\rm mod} = (\hat{b}_{\rm in}(\omega+\omega_{\rm d}),\ \hat{b}^{\dagger}_{\rm in}(\omega+\omega_{\rm d}),\ \hat{b}_{\rm in}(\omega-\omega_{\rm d}),\ \hat{b}^{\dagger}_{\rm in}(\omega-\omega_{\rm d}),\ \hat{a}_{\rm in}(\omega),\ \hat{a}^{\dagger}_{\rm in}(\omega),\ \hat{a}_{\rm in}(\omega+2\omega_{\rm d}),\ \hat{a}^{\dagger}_{\rm in}(\omega+2\omega_{\rm d}),\ \hat{a}_{\rm in}(\omega-2\omega_{\rm d}),\ \hat{a}^{\dagger}_{\rm in}(\omega-2\omega_{\rm d}))$ now comprises the shifted vectors. The iterative solution can be extended to include higher harmonics $\omega \pm n\omega_{\rm d}$ where $n = 3,\ 4$ ... since for very large ω_2, higher order sidebands become important. But in the present work, we limit ourselves to considering modest values of $\omega_2 \lesssim \omega_{\rm d}$ so we cut-off at $n = 2$; comparison with the full stochastic numerics were used to test convergence.

For convenience we first define the symbols

$$\begin{aligned}\mathcal{M}(\omega\pm\omega_{\rm d}) &= 1+\bar{g}^2\mu(\omega\pm\omega_{\rm d})\eta(\omega\pm2\omega_{\rm d})\\ \mathcal{N}(\omega) &= 1+\bar{g}^2\eta(\omega)(\mu(\omega+\omega_{\rm d})+\mu(\omega-\omega_{\rm d})).\end{aligned} \tag{25}$$

To represent the modifications to the mechanical susceptibilities due to second-order backactions. We also further define:

$$\begin{aligned}\mathcal{C}_1(\omega) &= \tilde{\chi}_{\rm M}(\omega+\omega_{\rm d})\tilde{\chi}_{\rm M}(\omega-\omega_{\rm d}),\\ \mathcal{C}_1^{\dagger}(\omega) &= \mathcal{C}_1^{*}(-\omega),\\ \mathcal{C}_{3\pm}(\omega) &= \tilde{\chi}_{\rm M}(\omega\pm\omega_{\rm d})\tilde{\chi}_{\rm M}(\omega\pm3\omega_{\rm d}),\\ \mathcal{C}_{3\pm}^{\dagger}(\omega) &= \mathcal{C}_{3\pm}^{*}(-\omega),\end{aligned} \tag{26}$$

where $\tilde{\chi}_{\rm M}(\omega) = \frac{\chi_{\rm M}(\omega)}{\mathcal{M}(\omega)}$ and $\tilde{\mu}(\omega) = \frac{\mu(\omega)}{\mathcal{M}(\omega)}$ are the modified susceptibilities.

We may conveniently split the vector of coefficients for $\hat{X}^{\pm}(\omega)$:

$$\vec{\mathcal{A}}_{X^{\pm}}(\omega) = \mathcal{N}^{-1}(\omega)[\vec{\mathcal{A}}'_{X^{\pm}}(\omega) - {\rm i}\omega_2\vec{\mathcal{G}}_{X^{\pm}}(\omega)] \tag{27}$$

into a vector, $\vec{\mathcal{A}}'_{X^{\pm}}$, corresponding to $\omega_2 = 0$ and another vector, $\vec{\mathcal{G}}_{X^{\pm}}(\omega)$ which comprises the terms dependent on ω_2.

In the main text, the shifted-displacement was expressed as a sum of thermal and backaction terms:

$$\begin{aligned}\hat{X}^{\pm}(\omega) &= \bar{g}\hat{Y}_{\rm BA}(\omega) - {\rm i}\omega_2\bar{g}\hat{Y}^{(\omega_2)}_{\rm BA}(\omega)\\ &\quad+\sqrt{\Gamma_{\rm M}}[\hat{X}_{\rm th}(\omega+\omega_{\rm d}) - \hat{X}_{\rm th}(\omega-\omega_{\rm d}) - {\rm i}\omega_2\hat{X}_{\omega_2}(\omega)].\end{aligned} \tag{28}$$

Below we give the thermal and backaction terms explicitly in terms of the noise vectors.

Thermal noise coefficients of $\hat{X}^{\pm}(\omega)$. For the thermal components in equation (28), we can write

$$\sqrt{\Gamma_{\rm M}}\,[\hat{X}_{\rm th}(\omega+\omega_{\rm d}) - \hat{X}_{\rm th}(\omega-\omega_{\rm d}) - {\rm i}\omega_2\hat{X}_{\omega_2}(\omega)] \equiv \mathcal{A}_{b_{\rm in}}(\omega+\omega_{\rm d})\hat{b}_{\rm in}(\omega+\omega_{\rm d}) + \mathcal{A}_{b_{\rm in}}(\omega-\omega_{\rm d})\hat{b}_{\rm in}(\omega-\omega_{\rm d}) + \mathcal{A}_{b_{\rm in}^{\dagger}}(\omega+\omega_{\rm d})\hat{b}_{\rm in}^{\dagger}(\omega+\omega_{\rm d}) + \mathcal{A}_{b_{\rm in}^{\dagger}}(\omega-\omega_{\rm d})\hat{b}_{\rm in}^{\dagger}(\omega-\omega_{\rm d}),$$

where the corresponding coefficients are given by:

$$\begin{aligned}\boldsymbol{\mathcal{A}}'_{b_{\rm in}}(\omega\pm\omega_{\rm d}) &= \pm\sqrt{\Gamma_{\rm M}}\,\tilde{\chi}_{\rm M}(\omega\pm\omega_{\rm d}),\\ \boldsymbol{\mathcal{A}}'_{b_{\rm in}^{\dagger}}(\omega\pm\omega_{\rm d}) &= \pm\sqrt{\Gamma_{\rm M}}\,\tilde{\chi}_{\rm M}^{*}(-(\omega\pm\omega_{\rm d}))\end{aligned} \tag{29}$$

and:

$$\begin{aligned}\boldsymbol{\mathcal{G}}_{b_{\rm in}}(\omega\pm\omega_{\rm d}) &= \mp\sqrt{\Gamma_{\rm M}}\,\mathcal{C}_1(\omega),\\ \boldsymbol{\mathcal{G}}_{b_{\rm in}^{\dagger}}(\omega\pm\omega_{\rm d}) &= \pm\sqrt{\Gamma_{\rm M}}\,\mathcal{C}_1^{\dagger}(\omega).\end{aligned} \tag{30}$$

We note that all the thermal noise terms scale with $\sqrt{\Gamma_{\rm M}}$; this means that whenever thermal processes are dominant the PSD spectra globally scale with $\Gamma_{\rm M}$: the shape of the functions $S_{xx}(\omega)$ and $S_{yy}(\omega)$ does not depend on $\Gamma_{\rm M}$, but their height and area scale linearly with $\Gamma_{\rm M}$.

Backaction terms in $\hat{X}^{\pm}(\omega)$. The incoming optical noise (here shot noise) drives fluctuations in the displacement which induces backaction noises in $\hat{X}^{\pm}(\omega)$.

The backaction terms in equation (28) are:

$$\bar{g}\hat{Y}_{\rm BA}(\omega) - {\rm i}\omega_2\bar{g}\hat{Y}_{\rm BA}^{(\omega_2)}(\omega) \equiv \mathcal{A}_{a_{\rm in}}(\omega)\hat{a}_{\rm in}(\omega) + \mathcal{A}_{a_{\rm in}^{\dagger}}(\omega)\hat{a}_{\rm in}^{\dagger}(\omega) + \mathcal{A}_{a_{\rm in}}(\omega+2\omega_{\rm d})\hat{a}_{\rm in}(\omega+2\omega_{\rm d}) + \mathcal{A}_{a_{\rm in}^{\dagger}}(\omega+2\omega_{\rm d})\hat{a}_{\rm in}^{\dagger}(\omega+2\omega_{\rm d}) + \mathcal{A}_{a_{\rm in}}(\omega-2\omega_{\rm d})\hat{a}_{\rm in}(\omega-2\omega_{\rm d}) + \mathcal{A}_{a_{\rm in}^{\dagger}}(\omega-2\omega_{\rm d})\hat{a}_{\rm in}^{\dagger}(\omega-2\omega_{\rm d}).$$

For which the corresponding coefficients:

$$\begin{aligned}\boldsymbol{\mathcal{A}}'_{a_{\rm in}}(\omega) &= -\bar{g}\,[\tilde{\mu}(\omega+\omega_{\rm d}) + \tilde{\mu}(\omega-\omega_{\rm d})]\,\sqrt{\kappa}\,\chi_o(\omega),\\ \boldsymbol{\mathcal{A}}'_{a_{\rm in}^{\dagger}}(\omega) &= -\bar{g}\,[\tilde{\mu}(\omega+\omega_{\rm d}) + \tilde{\mu}(\omega-\omega_{\rm d})]\,\sqrt{\kappa}\,\chi_o^{*}(-(\omega)),\end{aligned} \tag{31}$$

and:

$$\begin{aligned}\boldsymbol{\mathcal{G}}_{a_{\rm in}}(\omega) &= \bar{g}\mathcal{C}_1\sqrt{\kappa}\,\chi_o(\omega),\\ \boldsymbol{\mathcal{G}}_{a_{\rm in}^{\dagger}}(\omega) &= \bar{g}\mathcal{C}_1^{\dagger}\sqrt{\kappa}\,\chi_o^{*}(-\omega).\end{aligned} \tag{32}$$

Meanwhile, the backaction noise coefficients at $\omega\pm 2\omega_{\rm d}$ are:

$$\begin{aligned}\boldsymbol{\mathcal{A}}'_{a_{\rm in}}(\omega\pm 2\omega_{\rm d}) &= \bar{g}\tilde{\mu}(\omega\pm\omega_{\rm d})\,\sqrt{\kappa}\,\chi_o(\omega\pm 2\omega_{\rm d}),\\ \boldsymbol{\mathcal{A}}'_{a_{\rm in}^{\dagger}}(\omega\pm 2\omega_{\rm d}) &= \bar{g}\tilde{\mu}(\omega\pm\omega_{\rm d})\,\sqrt{\kappa}\,\chi_o^{*}(-(\omega\pm 2\omega_{\rm d}))\end{aligned} \tag{33}$$

and the corresponding ω_2 corrections are:

$$\begin{aligned}\boldsymbol{\mathcal{G}}_{a_{\rm in}}(\omega\pm 2\omega_{\rm d}) &= -\bar{g}\mathcal{C}_T\sqrt{\kappa}\,\chi_o(\omega\pm 2\omega_{\rm d}),\\ \boldsymbol{\mathcal{G}}_{a_{\rm in}^{\dagger}}(\omega\pm 2\omega_{\rm d}) &= -\bar{g}\mathcal{C}_T\sqrt{\kappa}\,\chi_o^{*}(-(\omega\pm 2\omega_{\rm d})),\end{aligned} \tag{34}$$

with $\mathcal{C}_T = (\mathcal{C}_1 + \mathcal{C}_1^{\dagger} + \mathcal{C}_{3\pm} + \mathcal{C}_{3\pm}^{\dagger})$.

For clarity, we present the † terms explicitly. They may also be given from $\boldsymbol{\mathcal{A}}'_{a_{\rm in}^{\dagger}}(\omega) = \boldsymbol{\mathcal{A}}'^{*}_{a_{\rm in}}(-\omega)$ etc; however the ${\rm i}\omega_2$ terms mean that extra care is needed.

Cavity output noise spectra

We can obtain the PSD of $\hat{X}^{\pm}(\omega)$ using the coefficients calculated above. Hence $\langle|x(\omega)|^2\rangle = S_{X^{\pm}X^{\pm}}$ is given by:

$$\begin{aligned}S_{X^{\pm}X^{\pm}}(\omega) = {} & (|\mathcal{A}_{b_{\rm in}}(\omega+\omega_{\rm d})|^2 + |\mathcal{A}_{b_{\rm in}}(\omega-\omega_{\rm d})|^2)\bar{n}_b\\ & + (|\mathcal{A}_{b_{\rm in}^{\dagger}}(\omega+\omega_{\rm d})|^2 + |\mathcal{A}_{b_{\rm in}^{\dagger}}(\omega-\omega_{\rm d})|^2)(\bar{n}_b+1)\\ & + |\mathcal{A}_{a_{\rm in}^{\dagger}}(\omega)|^2\\ & + |\mathcal{A}_{a_{\rm in}^{\dagger}}(\omega+2\omega_{\rm d})|^2 + |\mathcal{A}_{a_{\rm in}^{\dagger}}(\omega-2\omega_{\rm d})|^2,\end{aligned} \tag{35}$$

where we have used the noise correlators in equations (13) and (14) and assumed $\bar{n}_a = 0$.

The solutions to $\hat{X}^{\pm}(\omega)$ also enable us to easily construct equivalent vectors for the intracavity field and cavity output, including symmetrised spectra if desired, in terms of noises.

For example, the intracavity field $\hat{y}(\omega) = \frac{1}{\sqrt{2}}(\hat{a}(\omega) + \hat{a}^{\dagger}(\omega))$ is constructed by scaling the $\hat{X}^{\pm}(\omega)$ vector and adding the cavity-filtered incoming noise (equation (16)):

$$\hat{y}(\omega) = \bar{g}\eta(\omega)\hat{X}^{\pm}(\omega) + \sqrt{\kappa}\,\hat{Y}_{\rm in}(\omega). \tag{36}$$

Meanwhile, the cavity output amplitude is given by the standard relation $\hat{a}_{\rm out}(\omega) = \hat{a}_{\rm in}(\omega) - \sqrt{\kappa}\,\hat{a}$ and we consider the spectrum of its amplitude quadrature $\hat{y}_{\rm out}(\omega) = \frac{1}{\sqrt{2}}(\hat{a}_{\rm out}(\omega) + \hat{a}^{\dagger}_{\rm out}(\omega))$:

$$\hat{y}_{\rm out}(\omega) = \hat{y}_{\rm in}(\omega) - \sqrt{\kappa}\,\hat{y}(\omega). \tag{37}$$

We can write:

$$\hat{y}_{\rm out}(\omega) = \hat{I}(\omega) - \sqrt{\kappa}\bar{g}\eta(\omega)\hat{X}^{\pm}(\omega), \tag{38}$$

where $\hat{I}(\omega) = \hat{y}_{\rm in}(\omega) - \hat{Y}_{\rm in}(\omega)$ and $\hat{y}_{\rm in}(\omega) = \frac{1}{\sqrt{2}}(\hat{a}_{\rm in}(\omega) + \hat{a}^{\dagger}_{\rm in}(\omega))$. The cavity output PSD is then given in the form:

$$S_{y_{\rm out}y_{\rm out}}(\omega) = S_{\rm II}(\omega) + \kappa\bar{g}^2|\eta(\omega)|^2 S_{X^{\pm}X^{\pm}}(\omega) + \sqrt{\kappa}\bar{g}S_{IX^{\pm}}(\omega), \tag{39}$$

where $S_{\rm II}(\omega) = \langle\hat{I}^{\dagger}(\omega)\hat{I}(\omega)\rangle$ sets the imprecision noise floor and $S_{IX^{\pm}}(\omega) = 2{\rm Re}[\eta(\omega)\hat{I}^{\dagger}(\omega)X^{\pm}(\omega)]$ is the correlation of the displacement spectrum with imprecision noise.

Suppression of the $\omega_{\rm M} + \omega_{\rm d}$ sidebands

We can now analyse the suppression of the peaks at $\omega = \omega_{\rm M} + \omega_{\rm d}$ and at $\omega = -(\omega_{\rm M} + \omega_{\rm d})$ in $S_{y_{\rm out}y_{\rm out}}$ and S_{yy}. We can consider the asymmetry in the thermal regime where the sideband ratio r is invariant. In this case, we can neglect all the optical noise terms to simplify (equation (39)):

$$\frac{S_{y_{\rm out}y_{\rm out}}(\omega)}{\kappa\bar{g}^2|\eta(\omega)|^2} \approx (|\mathcal{A}_{b_{\rm in}}(\omega + \omega_{\rm d})|^2 + |\mathcal{A}_{b_{\rm in}}(\omega - \omega_{\rm d})|^2)\bar{n}_b + (|\mathcal{A}_{b^{\dagger}_{\rm in}}(\omega + \omega_{\rm d})|^2 + |\mathcal{A}_{b^{\dagger}_{\rm in}}(\omega - \omega_{\rm d})|^2)(\bar{n}_b + 1). \tag{40}$$

From this, we can obtain the sideband heights; for example, the height of the $\omega_{\rm M} + \omega_{\rm d}$ peak (correct up to a factor of n_b) is

$$|\mathcal{A}_{b_{\rm in}}(\omega - \omega_{\rm d})|^2 = |\tilde{\chi}_{\rm M}(\omega - \omega_{\rm d})|^2|1 - {\rm i}\omega_2\tilde{\chi}_{\rm M}(\omega + \omega_{\rm d})|^2, \tag{41}$$

the height of the $\omega_{\rm M} - \omega_{\rm d}$ peak is

$$|\mathcal{A}_{b_{\rm in}}(\omega + \omega_{\rm d})|^2 = |\tilde{\chi}_{\rm M}(\omega + \omega_{\rm d})|^2|1 - {\rm i}\omega_2\tilde{\chi}_{\rm M}(\omega - \omega_{\rm d})|^2, \tag{42}$$

and so on.

As in previous sections, note that all the susceptibilities $\tilde{\chi}_{\rm M}(\omega) = \frac{\chi_{\rm M}(\omega)}{\mathcal{M}(\omega)}$ are normalised by a factor $\mathcal{M}(\omega)$ arising from second-order backactions. This prevents unphysical spikes from emerging in the spectrum in the limit $\Gamma_{\rm M} \to 0$. Since we are operating in the thermal regime, we may omit these normalisations to get a simple reweighting of the thermal noise coefficients due to ω_2 correction.

$$|\mathcal{A}_{b_{\rm in}}(\omega \pm \omega_{\rm d})|^2 = |\chi_{\rm M}(\omega \pm \omega_{\rm d})|^2|1 - {\rm i}\omega_2\chi_{\rm M}(\omega \mp \omega_{\rm d})|^2. \tag{43}$$

The weighting factor $|1 - {\rm i}\omega_2\chi_{\rm M}(\omega \mp \omega_{\rm d})|^2$ can be seen as the ω_2 correction to the original height $|\chi_{\rm M}(\omega \pm \omega_{\rm d})|^2$.

The susceptibilities $\chi_{\rm M}(\omega \pm \omega_{\rm d})$ are sharply peaked at $\omega = \omega_{\rm M} \mp \omega_{\rm d}$, hence so is $\mathcal{A}_{b_{\rm in}}(\omega \pm \omega_{\rm d})$. Evaluating equation (43) at either $\omega = \omega_{\rm M} + \omega_{\rm d}$ or $\omega = \omega_{\rm M} - \omega_{\rm d}$, we find

$$|\mathcal{A}_{b_{\rm in}}(\omega_{\rm M} \pm \omega_{\rm d})|^2 = \frac{4}{\Gamma_{\rm M}^2}|1 - {\rm i}\omega_2\chi_{\rm M}(\omega_{\rm M} \mp 2\omega_{\rm d})|^2, \tag{44}$$

where

$$\chi_{\rm M}(\omega_{\rm M} \mp 2\omega_{\rm d}) = \frac{1}{\mp{\rm i}2\omega_{\rm d} + \frac{\Gamma_{\rm M}}{2}}. \tag{45}$$

Supposing that $\frac{\Gamma_{\rm M}}{2} \ll 2\omega_{\rm d}$, the sideband ratio is then

$$r = \frac{|\mathcal{A}_{b_{\rm in}}(\omega_{\rm M} - \omega_{\rm d})|^2}{|\mathcal{A}_{b_{\rm in}}(\omega_{\rm M} + \omega_{\rm d})|^2} \approx \frac{(2\omega_{\rm d} - \omega_2)^2}{(2\omega_{\rm d} + \omega_2)^2}. \tag{46}$$

Cavity output spectra in the quantum backaction limit

As seen previously and in the main text, in the limit $\Gamma_{\rm M} \to 0$, the thermal terms in equation (35) are negligible and $\hat{X}^{\pm}(\omega) \simeq \bar{g}Y_T(\omega)$ where the total backaction $Y_T(\omega) = \bar{g}\hat{Y}_{\rm BA}(\omega) - {\rm i}\omega_2\bar{g}\hat{Y}^{(\omega_2)}_{\rm BA}(\omega)$. In this case,

$$S_{X^{\pm}X^{\pm}} \approx (|\mathcal{A}_{a_{\rm in}^{\dagger}}(\omega + 2\omega_{\rm d})|^2 + |\mathcal{A}_{a_{\rm in}^{\dagger}}(\omega - 2\omega_{\rm d})|^2 + |\mathcal{A}_{a_{\rm in}^{\dagger}}(\omega)|^2). \quad (47)$$

The resulting backaction-dominated spectrum has the same asymmetry as the thermal spectrum: two peaks with height ratio r, as illustrated in figure 4(c) of the main text.

However, the cavity output spectrum includes also contributions arising from interference with incoming imprecision noise, thus terms like $\frac{\hat{Y}_{\rm imp}(\omega)}{\sqrt{\kappa}} - \bar{g}\hat{Y}_T(\omega)$ as shown in equation (7) ofthe main text. Equation (47) above exposes a new feature of the modulated system: there are backaction terms in dependent on $\omega \pm 2\omega_{\rm d}$ which are uncorrelated with $\hat{Y}_{\rm imp}(\omega)$ so cannot interfere with it. These terms are not present in standard (unmodulated) optomechanics.

In particular, if we split equation (47) into $S_{X^{\pm}X^{\pm}} = S_{Y_{\rm ba}} + S_{Y_{\rm ba2}}$ to differentiate ω and $\pm 2\omega_{\rm d}$ backactions, we can write the cavity output spectrum as:

$$S_{y_{\rm out}y_{\rm out}} = S_{\rm II} + \sqrt{\kappa}\bar{g}S_{IY_{\rm ba}} + \kappa\bar{g}^2|\eta(\omega)|^2(S_{Y_{\rm ba}Y_{\rm ba}} + S_{Y_{\rm ba2}Y_{\rm ba2}}). \quad (48)$$

While the terms $S_{Y_{\rm ba}Y_{\rm ba}} + S_{Y_{\rm ba2}Y_{\rm ba2}}$ give the same ratio as the thermal spectrum, the imprecision noise $S_{\rm II}$ plus the correlation term $S_{IY_{\rm ba}}$ changes the sideband ratio in the quantum limit.

Future experiments may elucidate further the novel form of the noise spectra of the modulated trap. Comparisons with nonlinear stochastic numerics validate the model in the classical regime, but do not include the non-commuting properties of the quantum noise spectra in equation (13) thus cannot test the model in the quantum limit.

References

[1] Aspelmeyer M, Kippenberg T J and Marquardt F 2014 *Rev. Mod. Phys.* **86** 1391
[2] Clerk A A, Devoret M H, Girvin S M, Marquardt F and Schoelkopf R J 2010 *Rev. Mod. Phys.* **82** 1155
[3] Teufel J D, Donner T, Li D, Harlow J H, Allman M S, Cicak K, Sirois A J, Whittaker J D, Lehnert K W and Simmonds R W 2011 *Nature* **475** 359
[4] Chan J, Mayer Alegre T P, Safavi-Naeini A H, Hill J T, Krause A, Groeblacher S, Aspelmeyer M and Painter O 2011 *Nature* **478** 89
[5] Verhagen E, Deleglise S, Weis S, Schliesser A and Kippenberg T J 2012 *Nature* **482** 63
[6] Marquardt F, Chen J P, Clerk A A and Girvin S M 2007 *Phys. Rev. Lett.* **99** 093902
[7] Wilson-Rae I, Nooshi N, Zwerger W and Kippenberg T J 2007 *Phys. Rev. Lett.* **99** 093901
[8] Braginsky V and Khalili F Y 1992 *Quantum Measurement* (Cambridge: Cambridge University Press)
[9] Safavi-Naeini A H, Chan J, Hill J T, Alegre T P M, Krause A and Painter O 2012 *Phys. Rev. Lett.* **108** 033602
[10] Khalili F Y, Miao H, Yang H, Safavi-Naeini A H, Painter O and Chen Y 2012 *Phys. Rev.* A **86** 033840
[11] Weinstein A J, Lei C U, Wollman E E, Suh J, Metelmann A, Clerk A A and Schwab K C 2014 *Phys. Rev.* X **4** 041003
[12] Peterson R W, Purdy T P, Kampel N S, Andrews R W, Yu P-L, Lehnert K W and Regal C A 2016 *Phys. Rev. Lett.* **116** 063601
[13] Safavi-Naeini A H, Groblacher S, Hill J T, Chan J, Aspelmeyer M and Painter O 2013 *Nature* **500** 185
[14] Purdy T P, Yu P L, Peterson R W, Kampel N S and Regal C A 2013 *Phys. Rev.* X **3** 031012
[15] Pontin A, Biancofiore C, Serra E, Borrielli A, Cataliotti F S, Marino F, Prodi G A, Bonaldi M, Marin F and Vitali D 2014 *Phys. Rev.* A **89** 033810
[16] Fonseca P Z G, Aranas E B, Millen J, Monteiro T S and Barker P F 2016 *Phys. Rev. Lett.* **117** 173602
[17] Jain V, Gieseler J, Moritz C, Dellago C, Quidant R and Novotny L 2016 *Phys. Rev. Lett.* **116** 243601
[18] Vovrosh J, Rashid M, Hempston D, Bateman J and Ulbricht H 2016 arXiv:1603.02917
[19] Mari A and Eisert J 2009 *Phys. Rev. Lett.* **103** 213603
[20] Malz D and Nunnenkamp A 2016 *Phys. Rev.* A **94** 023803
[21] Weis S, Riviere R, Deleglise S, Gavartin E, Arcizet O, Schliesser A and Kippenberg T J 2010 *Science* **330** 1520
[22] Yin Z-Q, Geraci A A and Li T 2013 *Int. J. Mod. Phys.* B **27** 1330018
[23] Romero-Isart O, Juan M L, Quidant R and Cirac J I 2010 *New J. Phys.* **12** 033015
[24] Chang D E, Regal C A, Papp S B, Wilson D J, Ye J, Painter O, Kimble H J and Zoller P 2010 *Proc. Natl Acad. Sci. USA* **107** 1005
[25] Monteiro T S, Millen J, Pender G A T, Marquardt F, Chang D and Barker P F 2013 *New J. Phys.* **15** 015001
[26] Kiesel N, Blaser F, Delić U, Grass D, Kaltenbaek R and Aspelmeyer M 2013 *Proc. Natl Acad. Sci. USA* **110** 14180
[27] Li T, Kheifets S and Raizen M G 2011 *Nat. Phys* **7** 527
[28] Gieseler J, Deutsch B, Quidant R and Novotny L 2012 *Phys. Rev. Lett.* **109** 103603
[29] Millen J, Fonseca P Z G, Mavrogordatos T, Monteiro T S and Barker P F 2015 *Phys. Rev. Lett.* **114** 123602